Available online at www.sciencedirect.com
SCIENCE DIRECT®
Journal of Power Sources 133 (2004) 329–336
JOURNAL OF POWER SOURCES
www.elsevier.com/locate/jpowsour

# Influence of pore structure on electric double-layer capacitance of template mesoporous carbons

Antonio B. Fuertes [a], Fernando Pico [b], Jose M. Rojo [b,*]

[a] *Instituto Nacional del Carbón, Consejo Superior de Investigaciones Científicas, La Correidoira, s/n, apartado 73, 33080 Oviedo, Spain*
[b] *Instituto de Ciencia de Materiales de Madrid, Consejo Superior de Investigaciones Científicas, Cantoblanco, 28049 Madrid, Spain*

Received 3 October 2003; received in revised form 12 February 2004; accepted 16 February 2004

**Abstract**

The behavior of two types of mesoporous carbons with different pore structures (i.e. unimodal and bimodal) as electrode material in an electrochemical double-layer capacitor has been analyzed. The carbon samples were prepared using mesostructured silica materials (MSM) as templating agents. The unimodal mesoporous carbon has a BET surface area of 1550 $m^2\,g^{-1}$, and a pore volume of 1.03 $cm^3\,g^{-1}$; the porosity is mainly made up of structural mesopores of ca. 3 nm that exhibit a narrow pore size distribution (PSD). The bimodal carbon shows larger surface area (1730 $m^2\,g^{-1}$) and larger pore volume (1.50 $cm^3\,g^{-1}$); the porosity is composed of two types of mesopores: structural (size around 3 nm) and complementary (size around 16 nm) mesopores. Both carbons show a disordered 3-D pore structure. Heat treatments at high temperatures (1000 °C) for long times (11 h) do not significantly change the pore structure with respect to the two synthesised carbons (800 °C). From the synthesized and heat-treated carbons, electrodes were processed as composites in which the carbons, polivinilidene fluoride (PVDF) and carbon black (CB) were the components. The effect of the heat treatment and relative CB content on specific capacitance, energy density and power density were studied. We found a specific capacitance of 200 $F\,g^{-1}$ for low current density (1 mA $cm^{-2}$) and 110 $F\,g^{-1}$ for high current density (150 mA $cm^{-2}$). Moreover, the curve of the specific capacitance versus current density shows three regimes, which are related to the three types of pore: micropores, structural mesopores and complementary mesopores. An energy density of 3 Wh $kg^{-1}$ at a power density of 300 W $kg^{-1}$ was obtained in some particular cases.


*Keywords:* Mesoporous carbon; Electrode material; Specific capacitance; ECDL capacitor; Supercapacitor

## 1. Introduction

Porous carbons have been widely employed as electrodes for energy storage in double-layer capacitors [1–9]. Normally active carbons have wide pore size distributions (PSDs) extending over the whole micropore–mesopore range (0–50 nm). However, it has been reported by several authors [2,7] that for this application, liquid electrolyte is not accessible to the narrow micropores. Only supermicropores (1–2 nm) and mainly mesopores (2–50 nm) serve for this purpose. Mesoporous carbons then are a good option for making electrode materials. However, the synthesis of carbons with a porosity made up almost exclusively from mesopores with sizes in a narrow range is unachievable following the classical methods of preparing active carbons [10]. A better way to prepare carbons with the aforementioned characteristics involves the use of inorganic materials as templates, whereby it is possible to obtain mesoporous carbons as inverse replicas [11]. This technique consists of: (i) impregnation of the inorganic porous structure (template) with a carbon precursor (generally a polymer or prepolymer), (ii) carbonization of the precursor inside the nanocomposite, and (iii) elimination of the template that gives rise to the pores. The mesoporous carbons show pore size and porosity that can be tailored over a wide range by choosing templates with specific structural characteristics. However, despite the interest on those carbons only a few examples of their use as electrodes for double-layer capacitors have been reported [12–14].

In general, carbon is good electrode material in which the capacitance, and hence the energy, comes from the electrochemical double layer formed at the carbon/electrolyte interface [1–9]. When the carbon particles are positively polarized, the negative ions of the electrolyte are situated near the carbon particles giving rise to the double layer. When the carbon is negatively polarized, the double layer

* Corresponding author. Tel.: +349-1334-9000; fax: +: +349-1372-0623.
*E-mail address:* jmrojo@icmm.csic.es (J.M. Rojo).

0378-7753/$ – see front matter © 2004 Elsevier B.V. All rights reserved.
doi:10.1016/j.jpowsour.2004.02.013

is formed with the positive ions of the electrolyte. The specific capacitance is linked to: (i) the electrical conductivity, the surface area and the porosity of the carbon, (ii) the accessibility of the electrolyte for penetrating into the carbon pores, and (iii) the electrolyte properties (mainly ionic conductivity, and size of the solvated ions). In relation with these parameters it should be pointed that the surface area and pore size distribution of the carbon on the one hand, and the electrical conductivity of the carbon on the other, seem to be the principal parameters that affect the energy and power of the electrochemical capacitor.

In this work we have synthesized two types of mesoporous carbons, one with pore size of ca. 3 nm (nearly unimodal carbon) and the other with pore sizes of ca. 3 and 16 nm (bimodal carbon); the size distribution is narrow for both pores. The samples were also heat-treated in an inert atmosphere to increase their electrical conductivity. From the synthesized and heat-treated carbons, electrodes were processed as composites to which PVDF, and in some cases CB, were added in different amounts. The electrochemical behavior of the electrodes was tested in capacitor cells. Dependence of specific capacitance versus current density has been analysed and discussed in terms of the two types of pores and the two types of samples. The energy density and power density were determined, and a comparison for the two types of samples (as-synthesized and heat-treated) is reported.

## 2. Experimental

### 2.1. Synthesis of mesoporous carbons

The synthesis of mesoporous carbons was carried out by means of a templating technique for which mesostructured silica materials (MSM) were chosen as templates. The MSM were prepared with the aid of non-ionic surfactants following the procedure previously reported by Zhao et al. [15]. An oligomeric alkyl-ethylene oxide surfactant $C_{16}EO_{10}$ (Brij 56, Aldrich) was used as the structure directing agent. Briefly, a silica source (TEOS, Aldrich) was added to an aqueous solution containing HCl and surfactant (Starting mole ratio, TEOS:Brij 56:HCl:$H_2O$ = 1:0.14:2:85). The mixture was magnetically stirred until the TEOS was dissolved. Then the mixture was placed in a closed Teflon vessel and stirred for 20 h at room temperature, followed by aging at 100 °C for 3 days. The precipitate was filtered, washed with distillate water, dried at 50 °C, and calcined in air to 600 °C (2 °C $min^{-1}$ heating rate) for 4 h. The yields were generally above 95% (based on silicon).

The carbons were prepared by impregnating the silica nanopores with a polymeric carbon precursor following the procedure reported elsewhere [16]. In a typical synthesis, the silica was impregnated with paratoluene sulfonic acid (0.5 M in ethanol). Afterwards, furfuryl alcohol was added to the silica until incipient wetness was achieved. The impregnated sample was cured in air for 12 h at 80 °C to polymerise the furfuryl alcohol and to convert it into polyfurfuryl alcohol, which was then carbonized under $N_2$ at 800 °C (2 °C $min^{-1}$ heating rate) for 1 h. The porous carbon was obtained after dissolution of the silica framework in 48 wt.% HF at room temperature. The resulting carbon sample contained only traces of silica (<1 wt.%). The carbon sample prepared in this way was denoted as B. The other carbon sample was obtained by carrying out the cycle of impregnation-curing-carbonisation twice. The resulting sample was denoted as U. Both carbons (B and U) were thermally treated under $N_2$ at 1000 °C for 11 h; the samples thus obtained are denoted as B-HT and U-HT.

In order to analyze the structural properties of the silica and carbon samples, nitrogen sorption isotherms were performed at −196 °C on a Micromeritics ASAP 2010 volumetric adsorption system. The BET surface area was deduced from the isotherm analysis in the relative pressure range of 0.04–0.20. The total pore volume was calculated from the amount adsorbed at a relative pressure of 0.99. The pore volume of structural mesopores and the external surface area were estimated using the $\alpha_s$-plot method. The reference adsorption data used for the $\alpha_s$ analysis of the silica and carbon samples correspond to a macroporous silica sample [17] and a nongraphitised carbon black (CB) sample [18], respectively. The PSD was calculated by means of the Kruk–Jaroniec–Sayari method [19] applied to the adsorption branch. The micropore volume of the carbon samples was estimated from the $CO_2$ adsorption isotherm measured on a gravimetric system (CI Electronics) at 20 °C. The Dubinin–Raduskevitch method was used to analyse the $CO_2$ adsorption data [20].

### 2.2. Electrical and electrochemical measurements

Electrodes were prepared as composites to which, polivinilidenefluoride (PVDF, MW ≈ 534 000) was added as an inert binder. In some particular cases where the composite showed high electrical resistance, carbon black supplied by MMM Carbon (Super P carbon black) was also added to decrease the resistance of the composite. The components of the composites were mixed and ground in an agate mortar. Then cylindrical pellets of diameter 13 mm, of thickness 0.6–0.8 mm, and of weight 50–80 mg were obtained after compaction at 38 MPa. The PVDF content was chosen as the minimum required to obtain handled pellets. This content was in the 10–40 wt.% range. The CB content was 5–10 wt.%.

The electrical conductivity of the electrodes was measured on parallelepipedic pellets that were compacted under the same pressure as the cylindrical pellets. Two-probe electrical measurements were carried out in a 1260 Solartron gain-phase analyzer (frequency range 5 Hz–1 MHz). When the resistance of the pellet was very low, four-probe electrical measurements were performed in line; a dc current was applied through the two external electrodes and the voltage drop was measured between the two internal electrodes. In

both procedures the electrodes were obtained from a silver paint. All measurements were carried out at room temperature.

Capacitors were assembled in two-electrode Swagelock-type cells, the cells being similar to those reported in reference [9]. Two equal cylindrical electrodes were separated by a glassy microfibre paper (934-AH Whatman) into which the liquid electrolyte (2 M $H_2SO_4$ aqueous solution) had been impregnated. Two tantalum rods served as current collectors. The charge and discharge of the capacitors was followed at room temperature with a 1286 Solartron potentiostat/galvanostat. The galvanostatic and voltammetric measurements were carried out in the current range of 1–200 mA and in the voltage scan rate range of 2–50 mV $s^{-1}$, respectively.

## 3. Results and discussion

### 3.1. Structural characteristics of mesoporous carbons

The structural characteristics of the mesostructure silica used as template are indicated in Table 1. This silica exhibits a 3-D disordered pore structure with a porosity made up of mesopores of approximately 4.1 nm and a wide PSD as evidenced by the value of the full-width at half-maximum (FWHM = 2.7 nm). The nitrogen sorption isotherm and the PSD of this sample are shown in Fig. 1a and b, respectively. A more detailed analysis of the structure of this material is given elsewhere [16].

The synthesized mesoporous carbons were obtained as inverse replicas of mesoporous silica. Consequently, they retained the structural characteristics of the silica used as template. In Table 1 the main structural properties of the synthesized carbons are outlined. The carbon (B sample) obtained in one impregnation-carbonization cycle clearly exhibits a bimodal pore system. This is deduced from the $N_2$ sorption isotherms (Fig. 1a, open circles), which contain two capillary condensation steps at relative pressures of ≈0.2 and ≈0.8. The PSD (Fig. 1b, open circles) clearly shows the existence of two pore systems, with sizes in the mesopore range centred at 2.9 and at ∼16 nm. The small mesopores (2.9 nm) derive from the removal of silica skeleta and are denoted as structural mesopores. The larger mesopores are originated from the coalescence of non-impregnated silica pores once the skeleta is removed; they are denoted as complementary mesopores. The pore volume assigned to complementary mesoporosity comprises around 65–70% that of the structural mesoporosity (see Table 1). An almost completely unimodal carbon (U sample) was obtained after two impregnation-carbonization cycles because the unfilled pores of the silica-carbon nanocomposite were impregated with the carbon precursor in the second cycle. The nitrogen sorption isotherm and the PSD of the synthesized U carbon are shown in Fig. 2a and b (open circles), respectively. This type of carbon mainly contains structural mesopores of size 2.8 nm that are similar to the structural mesopores of the B sample. Only a small portion of complementary mesopores of ca. 6–8 nm size remained in the U sample. The volume corresponding to the structural mesopores, as deduced from the α-plot analysis, is similar for both the U and B samples (Table 1); these mesopores are rather homogeneous in size as can be deduced from the narrow PSD peaks (FWHM ∼1 nm). The complementary mesopores show a wider range of sizes in both samples.

Micropore volumes estimated by $CO_2$ adsorption are in the 0.25–0.30 $cm^3\ g^{-1}$ range. These values coincide with the intrinsic microporosity reported for glassy carbons prepared from polyfurfuryl alcohol or phenolic resins by carbonisation at 1073 K and correspond to the inherent microporosity of the carbon framework.

The heat treatment at 1000 °C (11 h) to which the two carbons were subjected had no significant influence on their structural properties, as can be deduced from a comparison of the nitrogen sorption isotherms (Figs. 1a and 2a) and PSD (Figs. 1b and 2b) of the untreated B and U (open circles) and heat-treated B-HT and U-HT (closed circles) samples. The main found difference was that the heat treatment caused a slight shrinkage of the structural mesopores from 2.9 to 2.6 nm. The other structural parameters shown in Table 1 (i.e. BET surface area and pore volumes of structural and complementary pores) are not very different for the untreated

Table 1
Physical properties of mesostructured silica and templated carbons

| Sample | $S_{BET}$ ($m^2\ g^{-1}$) | $V_p$ ($cm^3\ g^{-1}$) [a] | $\alpha_s$-plot results | | $\delta_{KJS}$ (nm)[c] | FWHM (nm) [d] | Yield (g C $g^{-1}$ silica) |
|---|---|---|---|---|---|---|---|
| | | | $V_{mesop}$ ($cm^3\ g^{-1}$)[b] | $S_{ext}$ ($m^2\ g^{-1}$) | | | |
| Silica | 925 | 1.12 | 1.08 | 20 | 4.1 | 2.7 | – |
| B | 1730 | 1.50 | 0.86 (0.55) | 15 | 2.9 (15) | 1.1 | 0.54 |
| B-HT | 1810 | 1.37 | 0.74 (0.51) | 11 | 2.6 (16) | 1.5 | 0.54 |
| U | 1550 | 1.03 | 0.76 (0.18) | 6 | 2.8 | 1.0 | 0.68 |
| U-HT | 1540 | 0.94 | 0.66 (0.18) | 6 | 2.6 | 1.3 | 0.68 |

[a] Total pore volume from $N_2$ adsorption at $p/p_o = 0.99$.
[b] Volume of structural mesopores (i.e. derived from silica skeletal removal). The pore volume for complementary mesopores is given in brackets.
[c] Maximum of PSD. The size of larger mesopores is given in brackets.
[d] Full-width at half-maximum (FWHM) of structural mesopores.

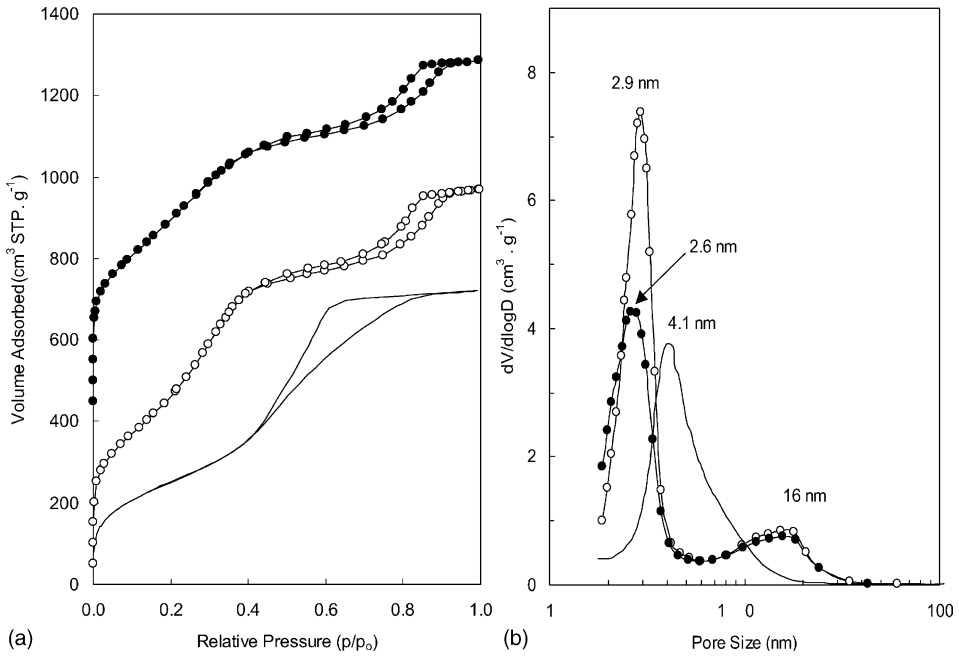


Fig. 1. Nitrogen sorption isotherms (a) and pore size distributions (b) of silica template (line) and derived bimodal carbons. The open and closed symbols stand for the non-treated (B) and 1000 °C-treated (B-HT) carbon, respectively.

B and U compared to the heat-treated B-HT and U-HT, respectively. This is in agreement with the results reported for other carbons [21].

### 3.2. Composites and their electrical conductivity

The electrodes were processed as composites from the samples U, U-HT, B and B-HT, according to a procedure described in the experimental section. In all cases PVDF was added to improve handling of the composite pellets. In some cases CB was also added because as CB is a good electronic conductor, its addition to the composite would increase the electrical conductivity of the composite. For this reason CB is usually added to the cathode composites of rechargeable lithium batteries, and its effect on the electrical conductivity and electrochem-

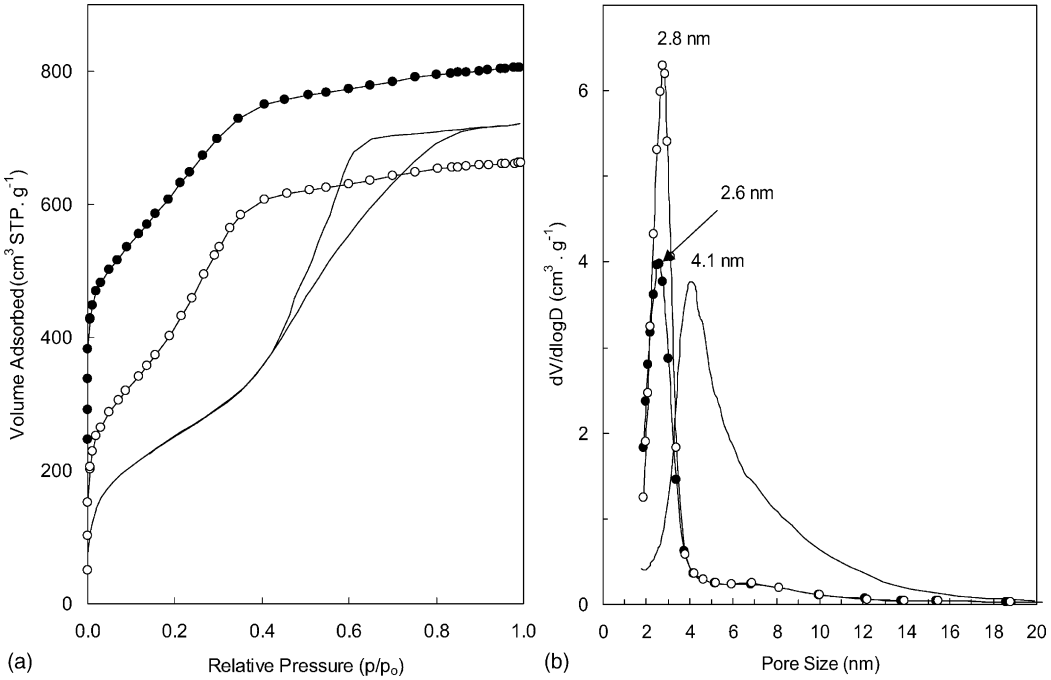


Fig. 2. Nitrogen sorption isotherms (a) and pore size distributions (b) of silica template (line) and nearly unimodal carbons. The open and closed symbols stand for the non-treated (U) and 1000 °C-treated (U-HT) carbon, respectively.

Table 2
Conductivity and resistance of the electrode composites

| Composition of the electrodes | Conductivity ($S\,cm^{-1}$) | Resistance (ohm) |
|---|---|---|
| 80 wt.% U + 20 wt.% PVDF | 0.013 | 5.0 |
| 75 wt.% U + 20 wt.% PVDF + 5 wt.% CB | 0.095 | 0.7 |
| 70 wt.% U + 20 wt.% PVDF + 10 wt.% CB | 0.32 | 0.2 |
| 80 wt.% U-HT + 20 wt.% PVDF | 0.19 | 0.3 |
| 60 wt.% B + 40 wt.% PVDF | 0.003 | 16 |
| 55 wt.% B + 40 wt.% PVDF + 5 wt.% CB | 0.042 | 1.5 |
| 90 wt.% B-HT + 10 wt.% PVDF | 0.24 | 0.2 |

ical behavior of the cathodes has been studied in detail [22].

The electrical conductivity of the electrodes as well as the resistance of the electrodes mounted in the capacitor cell are outlined in Table 2. The electrical conductivity was determined from electrical measurements. The resistance of the electrodes, however, was calculated from the conductivity and the geometrical dimensions of the electrodes. In the case of the electrodes based on the U sample it can be seen that: (i) the conductivity increases as the CB content increases and (ii) the conductivity of the electrode prepared with the U-HT sample is higher (about one order of magnitude) than that of the electrode prepared with the U sample. In the case of the electrodes based on the B and B-HT sample we find similar effects, i.e. the addition of CB increases the electrical conductivity of the composite and the electrodes made with the B-HT sample show a higher electrical conductivity than electrodes made with the B sample. Therefore, the heat treatment at 1000 °C increases the conductivity of the as-synthesized carbons. In addition, for the B sample, the heat treatment allowed us to obtain composite pellets with lower PVDF content (10 wt.% instead of 40 wt.%), and hence with higher content of active electrode material (90 wt.% instead of 55–60 wt.%).

### 3.3. Electrochemical characterization

The *I–V* curves obtained at three voltage scan rates on the capacitor with electrode material from the B-HT sample are shown in Fig. 3a. At $2\,mV\,s^{-1}$ (dot line) a near rectangular shape, which is characteristic of a capacitor can be observed. At $10\,mV\,s^{-1}$ the shape is also rectangular but slightly distorted (solid line). At $50\,mV\,s^{-1}$ the shape is clearly distorted (dashed line) because of the significant contribution of the equivalent series resistance (ESR) that is associated with the capacitor. This behavior has also been observed in other mesoporous carbons [12]. The *V–t* curves recorded in the galvanostatic experiments at two currents are shown in Fig. 3b. At the beginning of the charge and discharge we can see a sharp change in voltage ($\Delta V_1$), which is usually associated with the equivalent series resistance of the capacitor. In addition to this sharp voltage change, there is a gradual variation in voltage that increases for the charge and decreases for the discharge. From the voltage decrease ($\Delta V_2$) in the discharge we calculated the cell capacitance according to $C = I \times \Delta t_d / \Delta V_2$, where $\Delta t_d$ is the time spent during the discharge and I is the current. The capacitance of each electrode (Ce) can be calculated as Ce = 2 × C because both electrodes are in series arrangement within the capacitor cell. From the capacitance of each electrode and the mass of the carbon sample, the specific capacitance (in $F\,g^{-1}$) was calculated. We also estimated the capacitor efficiency as $(\Delta t_d / \Delta t_c) \times 100$, where $\Delta t_d$ and $\Delta t_c$ account for the discharge and charge time, respectively. Efficiencies of ca. 95% were found in all the analyzed capacitor cells.

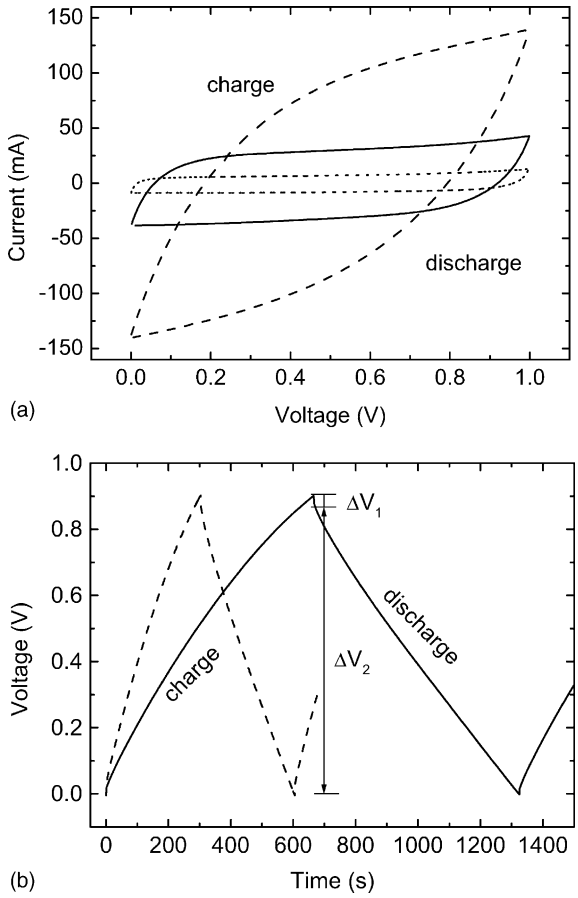


Fig. 3. (a) Voltammograms obtained at $2\,mV\,s^{-1}$ (dot line), $10\,mV\,s^{-1}$ (solid line), and $50\,mV\,s^{-1}$ (dashed line) for the capacitor cell having as electrodes the composite: 90 wt.% B-HT + 10 wt.% PVDF. (b) Galvanostatic curves recorded at 5 mA (solid line) and 10 mA (dashed line) in the same capacitor cell.

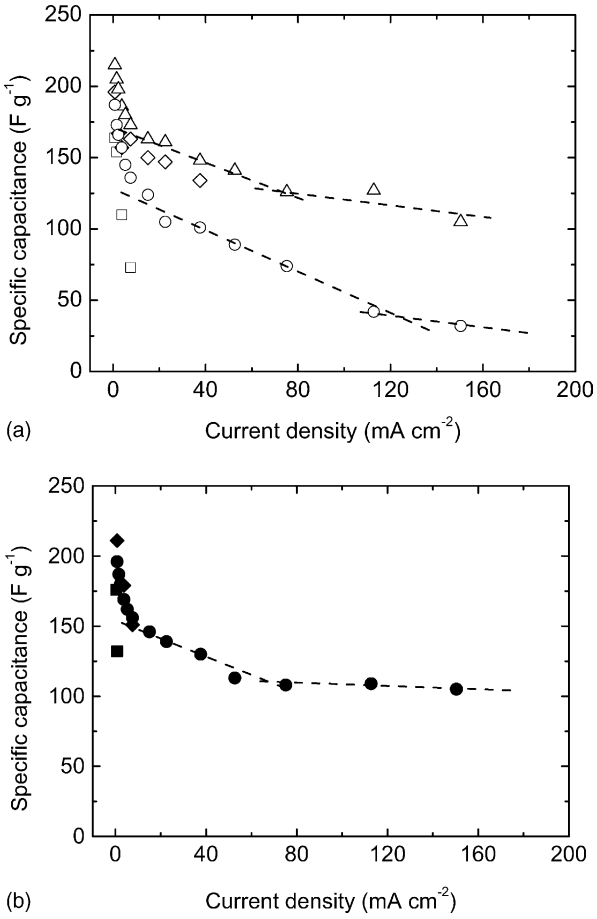


Fig. 4. Specific capacitance vs. current density. (a) The electrodes are composites with the following compositions: 80 wt.% U + 20 wt.% PVDF (open squares), 75 wt.% U + 20 wt.% PVDF + 5 wt.% CB (open diamonds), 70 wt.% U + 20 wt.% PVDF + 10 wt.% CB (open triangles), and 80 wt.% U-HT + 20 wt.% PVDF (open circles). (b) The electrodes show the compositions: 60 wt.% B + 40 wt.% PVDF (closed squares), 55 wt.% B + 40 wt.% PVDF + 5 wt.% CB (closed diamonds), and 90 wt.% B-HT + 10 wt.% PVDF (closed circles).

Variation in the specific capacitance versus current density is shown in Fig. 4. To ascertain whether the carbon black added to the electrode composite might have contributed to the capacitance measured, we measured the capacitance of a composite with only the CB and PVDF components. The capacitance obtained was so low compared to the capacitance of the composites with the U and U-HT samples, and also with the B and B-HT samples, that the capacitance of the electrodes could unambiguously be ascribed to the mesoporous carbon samples. In Fig. 4a we have plotted the specific capacitance for the U and U-HT samples. We can see that at low current density the specific capacitance is ca. 200 F $g^{-1}$ in all cases. Taking into account this value and the specific surface area (1540–1550 $m^2$ $g^{-1}$), we calculate a capacitance per area of 13 μF $cm^{-2}$, which agrees with the values usually reported for the double-layer capacitance (10–20 μF $cm^{-2}$). As the current density increases, the specific capacitance decreases, although behavior occurred in a different manner in each electrode. Thus, when the electrode was processed from the U sample and PVDF (without CB), the specific capacitance (open squares) decreased sharply, as the current density increased. However adding CB to the electrode changes the capacitance curve. In addition to the sharp decrease already mentioned, the capacitance decreases as the current density increases (open diamonds and triangles). It can be seen that the specific capacitance is slightly higher for the electrode with 10 wt.% CB (open triangles) than for the electrode with 5 wt.% CB (open diamonds). The specific capacitance of the U-HT sample is also shown in Fig. 4a (open circles). In this case where the composite had no CB, and in the case of the electrode prepared with the U sample and 10 wt.% CB (open triangles), the curve of the specific capacitance versus the current density shows three regimes: (i) a regime at current densities below 10 mA $cm^{-2}$ exhibiting high decrease ratio (ca. −11 F $g^{-1}$ $mA^{-1}$ $cm^2$), (ii) another regime at intermediate current densities (10–100 mA $cm^{-2}$) of lower ratio (ca. −0.8 F $g^{-1}$ $mA^{-1}$ $cm^2$), and (iii) another regime at higher current densities (above 100 mA $cm^{-2}$) where the ratio is even lower (ca. 0) and a nearly plateau can be observed. Three regimes are also found in the electrode prepared with the B-HT sample (Fig. 4b, closed circles). Therefore, they are observed when the electrodes show high electrical conductivity; it comes either from the heat treatment of the as-synthesized carbons or from addition of CB.

The three regimes are interpreted here on the basis of the pore structure of the mesoporous carbon samples. The regime (i) can be ascribed to the presence of micropores [2,4,23,24]. Because of the lower size of the micropores (mainly the micropores of 0–1 nm size) compared to the size of the hydrated ions of the electrolyte (hydrated $SO_4^{2-}$ and $H_3O^+$ in our case) [6,25], the double layer is formed with difficulty as the rate is increased. This fact accounts for the sharp decrease in capacitance observed. The regime (i) has also been observed in other microporous materials [26–28]. The regime (ii), at intermediate current densities, can be associated with the structural mesopores of our carbon samples. The same slope found in this regime for the electrodes made from the U, U-HT and B-HT samples agrees with the fact that in the three samples the structural mesopores are almost of the same size (2.6–2.9 nm) and exhibit similar narrow size distributions. The regime (iii), at high current densities, may be associated with the complementary mesopores that show a larger size and a wider size distribution. The external surface would also contribute to this regimes, but its contribution is not important as deduced from the low external surface (Table 1). In our view the slope of the specific capacitance and the pore size are associated as follows: the lower the slope in absolute value, the greater the pore size.

Since each regime is associated with a particular type of pore, a correlation between the specific capacitance (in F $g^{-1}$) of each regime and the volume of each pore type can be expected. These magnitudes and their percentages are outlined in Table 3 for the U, U-HT, and B-HT samples.

Table 3
Specific capacitance, pore volume, and their percentages corresponding to the micropores, structural mesopores, and complementary mesopores

| Electrode | Porosity | Specific capacitance | | Pore volume | |
|---|---|---|---|---|---|
| | | $F g^{-1}$ | % | $cm^3 g^{-1}$ | % |
| U + 10 wt.% CB | Micropores | 39 | 18 | 0.25 | 21 |
| | Structural mesopores | 61 | 28 | 0.76 | 64 |
| | Complemetary mesopores | 114 | 53 | 0.18 | 15 |
| U-HT | Micropores | 62 | 33 | 0.25 | 23 |
| | Structural mesopores | 95 | 50 | 0.66 | 61 |
| | Complementary mesopores | 30 | 16 | 0.18 | 16 |
| B-HT | Micropores | 39 | 20 | 0.30 | 19 |
| | Structural mesopores | 46 | 24 | 0.74 | 48 |
| | Complementary mesopores | 110 | 56 | 0.51 | 33 |

Although in the case of the U-HT sample there is an agreement between the percentages of the two magnitudes, no agreement is found for the other two samples. It seems that capacitance depends not only on the carbon sample but also on the processing of the electrode. Thus, while U and the U-HT show similar pore volumes for the micropores, structural mesopores and complementary mesopores, the capacitances associated with each type of pore for the electrode prepared with the U sample plus 10 wt.% of CB are different from those of the electrode made with the U-HT sample without CB (Table 3). A discussion similar can be made between the specific capacitance expressed in $F cm^{-3}$ and the pore volume. The former is easily calculated by dividing the specific capacitance (in $F g^{-1}$) by the pore volume (in $cm^3 g^{-1}$). However, for the specific capacitance expressed in $F cm^{-3}$, no better correlation between it and the pore volume has been found.

The Ragone plots for the U, U-HT, B, and B-HT samples are shown in Fig. 5. The energy ($W$) was calculated as $W = (1/2)C(\Delta V_2)^2$, where $C$ is the capacitance of the two-electrode capacitor cell and $\Delta V_2$ is the voltage decrease in the discharge. The power ($P$) was calculated as $P = W/\Delta t_d$, where $W$ is the energy and $\Delta t_d$ is the time spent in the discharge. The energy density and power density were calculated by dividing $W$ and $P$ by the mass of the mesoporous carbon sample in the capacitor cell. In Fig. 5 we can see that: (i) the energy density and power density of the U-HT (open circles) and B-HT (closed circles) are higher than those of the U (open squares) and B (closed squares) sample, respectively; the increment in power density being higher than in energy density, (ii) adding CB to the composite based on either the U (open diamonds and triangles) or the B (closed diamonds) sample, produces an increase in power density and energy density compared to the composites without CB (open squares and closed squares); the increment in power density is again higher than in energy density.

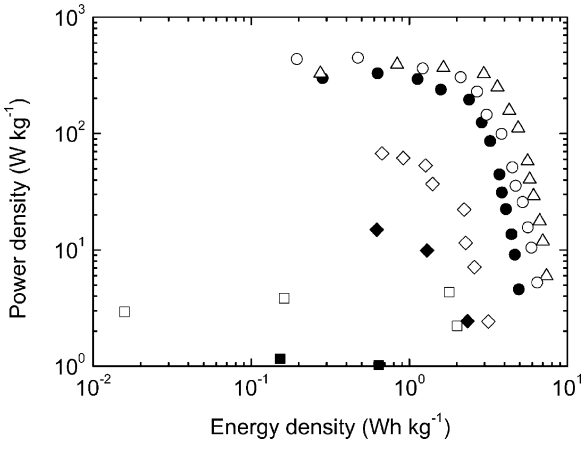


Fig. 5. Power density vs. energy density for the U, U-HT, B, and B-HT samples in the electrodes: 80 wt.% U + 20 wt.% PVDF (open squares), 75 wt.% U + 20 wt.% PVDF + 5 wt.% CB (open diamonds), 70 wt.% U + 20 wt.% PVDF + 10 wt.% CB (open triangles), 80 wt.% U-HT + 20 wt.% PVDF (open circles), 60 wt.% B + 40 wt.% PVDF (closed squares), 55 wt.% B + 40 wt.% PVDF + 5 wt.% CB (closed diamonds), and 90 wt.% B-HT + 10 wt.% PVDF (closed circles).

## 4. Conclusions

Mesoporous samples with narrow pore size distributions and high specific surface areas were obtained as inverse replicas of mesostructured silica materials, which were used as templates. By means of this technique two types of mesoporous carbons with approximately unimodal and bimodal pore size distributions were synthesized. Heating at 1000 °C in inert atmosphere does not significantly change the surface characteristics but increases the electrical conductivity of the samples. The energy density and power density of the heat-treated carbons are higher than those of synthesized carbons; the energy density and power density increase by one order of magnitude and two orders of magnitude, respectively. An energy density of ca. 3 Wh $kg^{-1}$ at a power density of ca. 300 W $kg^{-1}$ was found in one particular case. The current density dependence of the specific capacitance shows three regimes, which have been related with three types of pores: micropores, structural mesopores, and complementary mesopores.

## Acknowledgements

A.B.F. gratefully acknowledges the financial support provided for this research by the Spanish MCyT (MAT2002-00059). F.P. thanks the Red de Pilas de Combustible del CSIC for the fellowship received.

## References

[1] C. Niu, E.K. Sichel, R. Hoch, D. Moy, H. Tennent, Appl. Phys. Lett. 70 (1997) 1480.
[2] D. Qu, H. Shi, J. Power Sources 74 (1998) 99.
[3] H. Shi, Electrochim. Acta 41 (1999) 1633.
[4] B.E. Conway, Electrochemical supercapacitors, Kluwer Academic, New York, 1999 (Chapter 9 and 14).
[5] R. Kotz, M. Carlen, Electrochim. Acta 45 (2000) 2483.
[6] M. Endo, T. Takeda, Y.J. Kim, K. Koshiba, K. Ishii, Carbon Sci. 1 (2001) 117.
[7] E. Franckowiak, F. Beguin, Carbon 39 (2001) 937.
[8] K.H. An, W.S. Kim, Y.S. Park, Y.C. Choi, S.M. Lee, D.C. Chung, D.J. Bae, S.C. Lim, Y.H. Lee, Adv. Mater. 13 (2001) 497.
[9] Ch. Emmenegger, Ph. Mauron, P. Sudan, P. Wenger, V. Hermann, R. Gallay, A. Zuttel, J. Power Sources 124 (2003) 321.
[10] T. Kyotani, Carbon 38 (2000) 269.
[11] R. Ryoo, S.H. Joo, M. Kruk, M. Jaroniec, Adv. Mater. 13 (2001) 677.
[12] S. Yoon, J. Lee, T. Hyeon, M. Oh, J. Electrochem. Soc. 147 (2000) 2507.
[13] J. Lee, S. Yoon, S. Oh, C. Shin, T. Hyeon, Adv. Mater. 12 (2000) 359.
[14] H. Zhou, S. Zhu, M. Hibino, I. Honma, J. Power Sources 122 (2003) 219.
[15] D. Zhao, Q. Huo, J. Feng, B.F. Chmelka, D.G. Stucky, J. Am. Chem. Soc. 120 (2000) 6024.
[16] A.B. Fuertes, D.M. Nevskaia, Microp. Mesop. Mater. 62 (2003) 177.
[17] M. Jaroniec, M. Kruk, J.P. Oliver, Langmuir 15 (1999) 5410.
[18] M. Kruk, M. Jaroniec, K.P. Gadkaree, J. Colloid Interface Sci. 192 (1997) 250.
[19] M. Kruk, M. Jaroniec, A. Sayari, Langmuir 13 (1999) 6267.
[20] F. Stoeckli, in: J W Patrick (Ed.), Characterisation of Microporous Carbons by Adsorption and Inmersion Techniques, Porosity in Carbons, Edward Arnold, London, 1995 (Chapter 3).
[21] C. Lin, J.A. Ritter, B.N. Popov, J. Electrochem. Soc. 146 (1999) 3639.
[22] S. Mandal, J.M. Amarilla, J. Ibáñez, J.M. Rojo, J. Electrochem. Soc. 148 (2001) A24.
[23] S. Shiriaishi, H. Kurihara, A. Oya, Carbon Sci. 1 (2001) 133.
[24] B.E. Conway, W.G. Pell, J. Power Sources 105 (2002) 169.
[25] M. Endo, T. Maeda, T. Takeda, Y.J. Kim, K. Koshiba, H. Hara, M.S. Dresselhaus, J. Electrochem. Soc. 148 (2001) A910.
[26] H.Y. Lee, V. Manivannan, J.B. Goodenough, C.R. Acad. Sci. Paris 2 (1999) 565.
[27] Y.U. Jeong, A. Manthiram, J. Electrochem. Soc. 148 (2001) A189.
[28] J. Zhang, D. Jiang, B. Chem, J. Zhu, L. Jiang, H. Fang, J. Electrochem. Soc. 148 (2001) A1362.